Interface Focus

CrossMark
click for updates

Interface Focus (2012) **2**, 645–650
doi:10.1098/rsfs.2011.0091
Published online 1 February 2012

Electromagnetic characterization of millimetre-scale replicas of the gyroid photonic crystal found in the butterfly *Parides sesostris*

C. Pouya* and P. Vukusic

School of Physics, University of Exeter, Exeter EX4 4QL, UK

We have used three-dimensional stereolithography to synthetically replicate the gyroid photonic crystal (PC) structure that occurs naturally in the butterfly *Parides sesostris*. We have experimentally characterized the transmission response of this structure in the microwave regime at two azimuthal angles (ϕ) over a comprehensive range of polar angles (θ). We have modelled its electromagnetic response using the finite-element method (FEM) and found excellent agreement with experimental data. Both theory and experiment show a single relatively broad transmission minimum at normal incidence ($\theta = 0^\circ$) that comprises several narrow band resonances which separate into clearly identifiable stop-bands at higher polar angles. We have identified the specific effective geometric planes within the crystal, and their associated periodicities that give rise to each of these stop-bands. Through extensive theoretical FEM modelling of the gyroid PC structure, using varying filling fractions of material and air, we have shown that a gyroid PC with material volume fraction of 40 per cent is appropriate for optimizing the reflected bandwidth at normal incidence (for a refractive index contrast of 1.56). This is the same gyroid PC material volume fraction used by the butterfly *P. sesostris* itself to produce its green structurally coloured appearance. This infers further optimization of this biological PC beyond that of its lattice constant alone.

Keywords: *Parides sesostris*; gyroid; photonic crystal; self-assembly

1. INTRODUCTION

Many natural systems have evolved photonic structures at optical length scales to interact with light in order to produce vivid colour appearances [1], iridescence [2], polarization effects [3,4], and even blackness [5] and whiteness [6,7]. Although nature is able to self-assemble organic materials to create these structures, traditional technological fabrication methods have suffered from resolution limitations that prevent the fabrication of extremely intricate structures similar to the natural systems. Advances in processes such as direct laser writing are producing increasingly improved resolution limits that provide the prospect for future sample fabrication of extremely intricate structures at near infrared [8] and optical length scales [9]. Other fabrication methods for the production of optical photonic structures that are currently progressing the field, including stacking processes [10], self-assembly [11], novel methods of biotemplating naturally occurring optical photonic structures [12] and lithography techniques [13]. The scalability of Maxwell's equations allows us to probe larger photonic structures in longer wavelength regimes that facilitate experimental determination of the electromagnetic response of analogous smaller optical structures. Three-dimensional printing, using stereolithography principles, is a fabrication technique suitable for creating complex three-dimensional photonic structures. It has previously been used for fabricating and measuring the electromagnetic response of synthetic quasi-ordered photonic crystals (PCs) [14] and of large-scale replicas of simpler butterfly photonic structures in the microwave regime [15]. With this fabrication technique, even very complex physical structures—comprising elaborate geometries—can be manufactured to possess resonant transmission/reflection frequencies that lie comfortably within an experimentally accessible microwave frequency range. In this instance, the sample fabrication resolution, of approximately 50 μm, is not an obstacle to the use of millimetre-scale lattice constants and interrogation wavelengths.

An interesting group of crystal structures is known as the bicontinuous cubic structure group: these contain two interconnecting channels comprising different materials that exhibit periodicity in three dimensions [16]. The intermediate surface which separates the two channels is often a minimal surface [16,17], in which case they are often referred to as triply periodic minimal surfaces (TPMS). There are three fundamental bicontinuous cubic structures; these are based on simple cubic, face-centred cubic and body-centred cubic Bravais lattice systems [16]. The corresponding minimal

*Author for correspondence (c.pouya@ex.ac.uk).

One contribution of 18 to a Theme Issue 'Geometry of interfaces: topological complexity in biology and materials'.

Received 1 October 2011
Accepted 6 January 2012

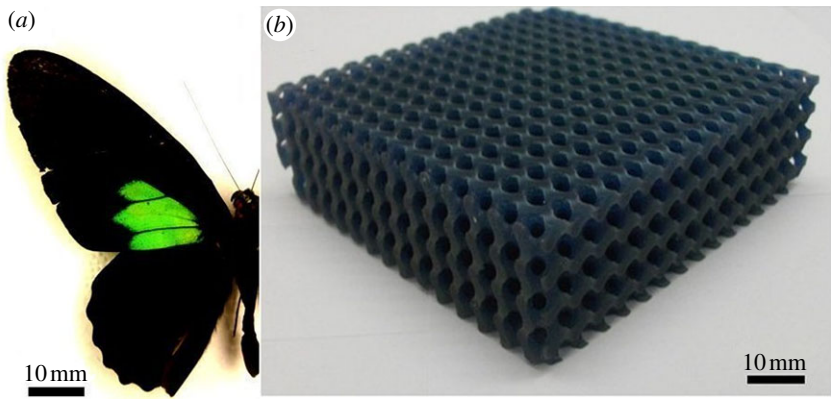

Figure 1. (*a*) *Parides sesostris*: the green regions are produced by scales that contain a gyroid photonic crystal structure. (*b*) The fabricated gyroid sample with 40% material ($n = 1.656$) and 60% air. Lattice constant is 7 mm.

surfaces that define their geometry are labelled as the P, D and G surfaces, respectively. Minimal surfaces are naturally formed via self-assembly of two materials: for instance, mixing lipids and water with the use of surfactants in chemical mixing processes [17]. The G surface or 'gyroid' has recently been the subject of great interest, particularly as a PC structure in the biological world [16,18–20]. Several butterflies, including *Parides sesostris* (figure 1*a*), were previously thought to contain various inverse opal type PC structures of air spheres in a cuticle matrix [21,22]. A recent study [16], using an iterative image analysis process [16,21], has shown these butterfly samples, in fact, contain the gyroid bicontinuous cubic structure [16]. The gyroid is often thought of as the most commonly appearing TPMS [17]. This suggests its formation, via self-assembly, can be particularly energetically favourable. In terms of self-assembly-driven synthetic manufacture of PCs at optical length scales, this is an appealing attribute. Furthermore, the existence of two chiral axes in the gyroid yields unusual polarization properties such as circular dichroism [19].

Previously, only theoretical modelling attempts have been undertaken with respect to characterizing the detailed polarization- and orientation-dependent electromagnetic response of the gyroid PC. Those that have been published have featured only normal incidence analysis [19,23]. Until our investigation, no experimental data have existed for a full characterization of the electromagnetic response of a gyroid PC coupled to a direct comparison with appropriate theory for the same structure. Our vehicle for realizing this involved the fabrication of a scaled-up replica (figure 1*b*) of the gyroid PC structure found in the butterfly (*P. sesostris*; figure 1*a*) using the rapid-prototyping stereolithography method. We manufactured the replica with the same filling fraction (FF) as that found in the gyroid PC of *P. sesostris* (40% material, 60% air [16]) in order to mimic its electromagnetic response at microwave wavelengths. We have experimentally taken a comprehensive range of angle- and polarization-dependent data from our fabricated gyroid structure. These data were then compared with the theoretical modelling for the identical structure using finite-element method (FEM). In addition to this experimental and theoretical characterization of the gyroid PC which best represents the butterfly's authentic structure, we also undertook further modelling that involved systematically varying the FF of the PC structure. The aim of this was to determine whether *P. sesostris*' gyroid possesses an optimal FF in relation to the refractive index of material used.

2. MICROWAVE EXPERIMENTAL METHODS AND THEORETICAL MODELLING

We used three-dimensional computer-aided design software SOLIDWORKS (http://www.solidworks.com) alongside the three-dimensional surface-creating software K3DSURF (v. 0.6.2. Abderrahman Taha) to fabricate a synthetic three-dimensional gyroid structure comprising 40 per cent (material) and 60 per cent (air). We used a Pro Jet HD 3000 stereolithography machine to fabricate a three-dimensional model of the structure with a lattice constant of 7 mm (figure 1*b*). This method produces structures created from a polymer with a refractive index of $n = 1.65$ (measured using established techniques [24]). The gyroid from the butterfly has a lattice constant of $a = 260 \pm 63$ nm [16]. The 7 mm lattice constant was chosen, so that the principle electromagnetic transmission features associated with the gyroid structure were located in the frequency range 10–43 GHz. This coincided with the best working frequency range of the broadband source and detector that were subsequently used to conduct the experiment (Flann model DP241-AB; dual-polarized horn; option 10–50 GHz). The sample size of the three-dimensional printed structure was chosen to be $15 \times 15 \times 4$ unit cells, which was suitable for the incident beam-spot area. The fabricated gyroid structure was designed so that the interface on which microwaves were incident was parallel to the (001) plane of the gyroid. Our experimental apparatus consisted of an emitting and a receiving broadband horn attached to an Anritsu Vector Star 70 kHz to 70 GHz vector network analyser. The sample was centred between aligned source and detector horns. We surrounded the sample with microwave absorber to ensure the radiation transmitted only through the structure was collected by the receiving horn. We performed transmission experiments, using both transverse magnetic (TM) and transverse electric (TE) polarizations, on the structure at two azimuthal angles $\phi = 0^\circ$ and $\phi = 45^\circ$. In

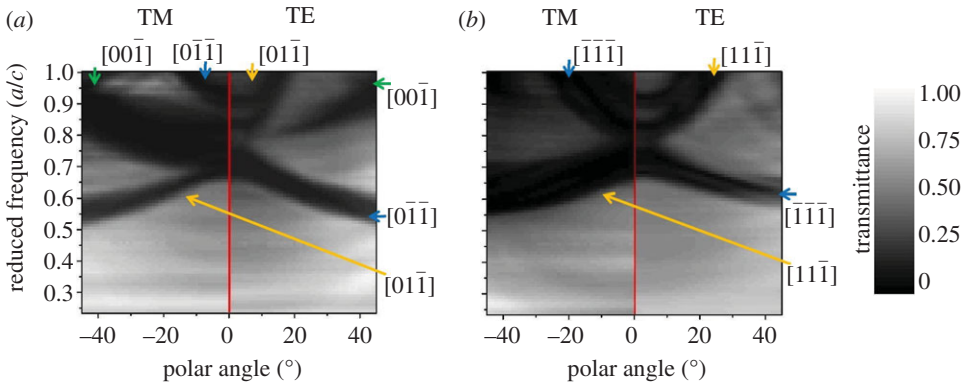

Figure 2. Experimental transmission data taken from the synthetically fabricated gyroid structure in the microwave regime, presented in reduced frequency units taken at an azimuthal angle (ϕ) of (*a*) 0° and (*b*) 45°. The sample was rotated over a comprehensive polar angular (θ) range. The negative values of polar angle represent experimental data taken with TM-polarized radiation, and the positive values represent experimental data taken with TE-polarized radiation. Miller indices indicate the directions through the crystal for which there exist periodicities of effective planes of the gyroid.

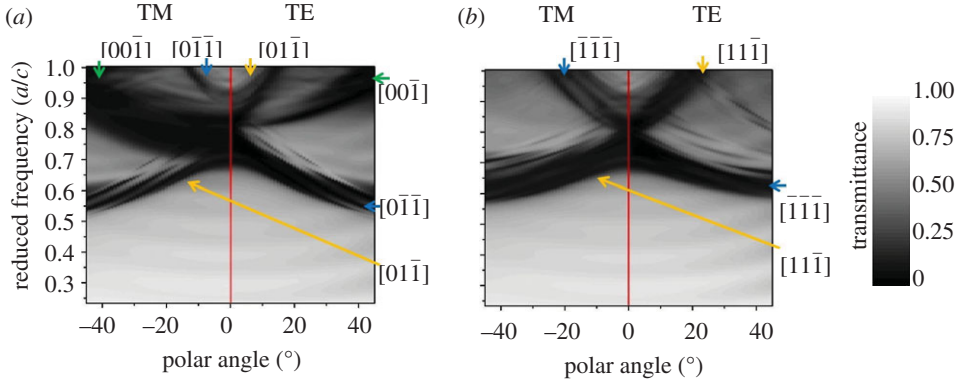

Figure 3. Theoretical transmission data taken from using finite-element method modelling in the microwave regime, presented in units of reduced frequency. Polar angular data taken at an azimuthal angle of (*a*) 0° and (*b*) 45°. The theoretical model replicated the physical model. The data are presented in the same format as the experimental data in figure 2.

each case, the sample was rotated through a polar angle range $-45^\circ \leq \theta \leq 45^\circ$.

We theoretically modelled the response of the gyroid structure using an FEM model [25]. Our model geometry replicated the experimental model as an infinite array that was four unit cells deep. The same lattice constant, refractive index contrast and packing fraction were used in both the experimental and the theoretical model.

To explore whether the optical gyroid in *P. sesostris* is optimized with respect to FF, we ran further simulations in which the material FF of the model was varied from 26 per cent ≤ material volume ≤ 74 per cent, at normal incidence. This FF is determined by a corresponding value of '*t*' which forms part of the general surface equation of the gyroid. Both the theoretical and replica gyroids were produced using the technique described by Wohlgemuth *et al.* [26] for generating the gyroid's three-dimensional minimal surface. An equation, which defines this surface is

$$\sin\left(\frac{2\pi x}{a}\right)\cos\left(\frac{2\pi y}{a}\right)+\sin\left(\frac{2\pi y}{a}\right)\cos\left(\frac{2\pi z}{a}\right)+\cos\left(\frac{2\pi x}{a}\right)\sin\left(\frac{2\pi z}{a}\right)=t,$$

where x, y and z are spatial coordinates, and a is the lattice constant. The parameter 't' determines the volume fraction of each of the interconnecting channels, and therefore, the FF of the gyroid PC [16,23]. For this optimization modelling, we systematically varied t from $-0.7 \leq t \leq 0.7$ (i.e. 26% ≤ material volume ≤ 74%).

3. RESULTS AND DISCUSSION

Figure 2*a*,*b* shows the experimental data representing the TM and TE transmission response at $\phi = 0^\circ$ and at $\phi = 45^\circ$ of the gyroid replica. There is excellent agreement between experimental data (figure 2*a*,*b*) and theoretical modelling (figure 3*a*,*b*). At normal incidence ($\theta = 0^\circ$), the regions of low transmission (and therefore high reflection) in these plots lie close together in frequency and appear as one broadband feature. They then separate into several unique bands at non-normal polar angles. In the reduced frequency range from 0.233 to 1, the data in figures 2 and 3 reveal stop-bands associated with transmission minima over the evaluated angle ranges. The physical origin of each stop-band can be deduced from the nature of the dispersion with angle of each low-transmission

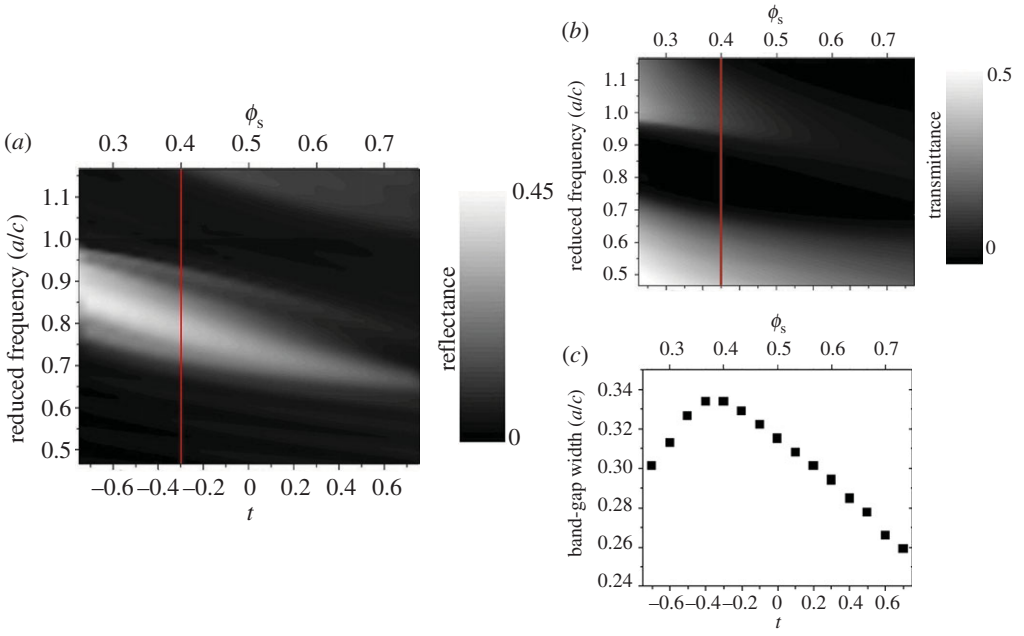

Figure 4. Theoretical modelling of (*a*) the reflection and (*b*) transmission response of the gyroid structure with varying filling fraction (FF; shown as a function of t—a parameter taken from the surface equation of the gyroid and also ϕ_s—the material volume FF). The red lines indicate the parameter of t, and the FF, of the gyroid photonic crystal structure found in the butterfly *P. sesostris*. (*c*) Band-gap width as a function of FF.

stop-band in addition to the time-averaged electric fields calculated and visualized using the theoretical model at individual frequencies. The stop-band resonances arise from periodicities that originate from the distinct sets of effective structural planes that exist within this three-dimensional PC. The stop-bands in figures 2 and 3 are labelled with the Miller indices that correspond to the vector directions in which the periodicities occur. The $[00\bar{1}]$ band increases in frequency as polar angle (θ) is increased; this is characteristic of a set of planes that are aligned parallel to the sample surface. However, the $[0\bar{1}\,\bar{1}]$, $[01\bar{1}]$, $[11\bar{1}]$ and $[\bar{1}\,\bar{1}\,\bar{1}]$ bands have periodic effective planes that are oriented at 45° to the surface of the sample. In these cases, the stop-bands decrease in frequency as the angle of incident radiation approaches the normal to each effective plane of the gyroid, and increases in frequency when the angle of incident radiation moves away from the normal of each effective plane. Figures 2 and 3 show these characteristic bands. The resonance that occurs strongly in the $[00\bar{1}]$ direction in the $\phi = 0°$ case does occur in the $\phi = 45°$ case, but is very weak in comparison. This represents a much more intense reflection from these periodic planes for $\phi = 0°$ compared with $\phi = 45°$.

In order to test whether the gyroid structure (corresponding to 40% material and 60% air [16]) within *P. sesostris* is optimized beyond the variable of lattice constant alone, we modelled the reflectance and transmittance of the gyroid PC constructed using a series of different FFs. Figure 4 shows the collective results of this systematic variation of FF for the gyroid PC over the range $-0.7 \leq t \leq 0.7$ ($26\% \leq$ material volume $\leq 74\%$). The refractive index of the material was kept constant. Figure 4 comprises graphs of theoretical modelling that show the variation of reflectance (figure 4*a*), transmittance (figure 4*b*) and the width of the band-gap (figure 4*c*) over the evaluated range of FF. These data indicate a clear region of the widest reflected bandwidth associated with FFs in the t-interval $-0.4 \leq t \leq -0.2$, and the material volume fraction of $0.37 \leq \phi_s \leq 0.43$. The actual corresponding FF associated with *P. sesostris* lies in the centre of this range with a value of $t = -0.3$ ($\phi_s = 0.4$) [16]. We reason that this is an adapted design feature of *P. sesostris* because it creates the effect of the widest possible reflection bandwidth for the butterfly's PC structure. Usually, a large stop-band width and a full and complete band-gap are features of PCs that have high inherent refractive index contrasts [27]. The lowest possible refractive index contrast, for an ordered PC structure, that will yield a full and complete band-gap is produced by the diamond PC, and has a value of approximately 2 [28]. This limit of refractive index contrast cannot be met by this butterfly's compositional materials. The natural material available to all butterflies including *P. sesostris*, namely insect cuticle, only has a relatively low refractive index of $n = 1.56$ [29] which it uses alongside air. While it cannot improve this refractive index contrast, it appears to have compensated for it by producing a PC with the specific FF that maximizes the stop-band width.

As the transmission spectra in figures 2 and 3 were taken from a gyroid with the same FF as *P. sesostris*, we can discuss this broadband effect on the overall electromagnetic response. As this FF maximizes the widths of each band, we observe that in figures 2*a* and 3*a* the TM $[00\bar{1}]$ band has regions of the same frequency in the stop-band over angles $\theta = -45°$ to $\theta = 0°$. This is also the case in figures 2*b* and 3*b* for the lower $[\bar{1}\,\bar{1}\,\bar{1}]$ and $[11\bar{1}]$ bands. The extent of overlap of frequencies in these stop-bands over the 45° angle range will be reduced or may not be present at all if any other FF was used. This is a further indicator that *P. sesostris*

has used an optimized FF in order to maximize the bandwidth of reflected light. The optical effect it provides is a suppression of iridescence, namely reduced angle-dependence of the reflected structural colour. Iridescence suppression has also been attributed to several other obvious structural embellishments of *P. sesostris*, not related to FF [30,31]. Another example of FF optimization was previously also shown in a different biological photonic system with a two-dimensional structure [32].

4. CONCLUSION

We have modelled and experimentally gathered a range of angle-dependent transmission data for a gyroid PC structure at microwave frequencies using both TE- and TM-polarized incident radiation. This gyroid structure, including its FF, was designed to replicate the gyroid found in the scales of the structurally coloured butterfly *P. sesostris*. This was performed at the millimetre-scale to enable extensive experimental electromagnetic characterization, something which is difficult to achieve with the sub-micrometre-size structure of the actual butterfly itself. To do this, we used the scalability of Maxwell's equations and fabricated the synthetic sample with dimensions suitable for characterization in the microwave regime. We undertook concurrent theoretical analysis using models created with the same software tools that were used for the fabrication of the synthetic model itself. Our results (figures 2 and 3) showed excellent agreement between theory and experiment. We have identified the effective geometric planes of the gyroid PC that are responsible for the resonances observed experimentally and modelled theoretically. This was achieved by considering the gyroid's compositional effective structural planes and how they influence the incident electromagnetic radiation on rotation.

In addition to this, we have also theoretically analysed the effect of varying FF of the gyroid PC structure on its reflection response. We have shown that *P. sesostris*' PC FF appears optimized to produce a maximum reflected bandwidth for the refractive index of the materials with which it is formed (chitin, $n = 1.56$, and air). Ordered PCs are generally iridescent, and so the reflected colour is angle-dependent. This can generally be minimized by increasing the reflected bandwidth, so the shift in wavelength allows certain wavelengths to be reflected over all angles. Because large bandwidths are usually associated with PCs that have a high refractive index contrast, something that is inaccessible to *P. sesostris*, we suggest it exploits a highly tuned FF to enhance its reflected bandwidth, consequently minimizing the angle-dependence of its reflected colour.

Parides sesostris uses many other mechanisms to create angle-independent colour reflection, such as PC domaining [31,32] and a scale-surface ridge structure that appears to diffuse reflected light. An optimized FF has been previously overlooked as another mechanism that contributes to the extremely well-designed configuration for manipulating light in an angle-independent manner while using low refractive index contrast media.

The authors thank D.G. Stavenga for helpful discussion. Financial support was given by AFOSR/EOARD grant no. FA8655-08-1-3012 and AFOSR grant no. FA9550-10-1-0020, and by the School of Physics at the University of Exeter.

REFERENCES

1 Kinoshita, S., Yoshioka, S., Fujii, Y. & Okamoto, N. 2002 Photophysics of structural color in the Morpho butterflies. *Forma* **17**, 103–121.
2 Seago, A. E., Brady, P., Vigneron, J. P. & Schultz, T. D. 2009 Gold bugs and beyond: a review of iridescence and structural colour mechanisms in beetles (Coleoptera). *J. R. Soc. Interface* **6**(Suppl. 2), S165–S184. (doi:10.1098/rsif.2008.0354.focus)
3 Jewell, S. A., Vukusic, P. & Roberts, N. W. 2007 Circularly polarized colour reflection from helicoidal structures in the beetle *Plusiotis boucardi*. *New J. Phys.* **9**, 99. (doi:10.1088/1367-2630/9/4/099)
4 Sharma, V., Crne, M., Park, J. O. & Srinivasarao, M. 2009 Structural origin of circularly polarized iridescence in jeweled beetles. *Science* **325**, 449–451. (doi:10.1126/science.1172051)
5 Vukusic, P., Sambles, J. R. & Lawrence, C. R. 2004 Structurally assisted blackness in butterfly scales. *Proc. R. Soc. Lond. B* **271**(Suppl. 4), S237–S239. (doi:10.1098/rsbl.2003.0150)
6 Vigneron, J. P., Rassart, M., Vértesy, Z., Kertész, K., Sarrazin, M., Biró, L. P., Ertz, D. & Lousse, V. 2005 Optical structure and function of the white filamentary hair covering the edelweiss bracts. *Phys. Rev. E Stat. Nonlin. Soft Matter Phys.* **71**, 011906. (doi:10.1103/PhysRevE.71.011906)
7 Vukusic, V., Hallam, B. & Noyes, J. 2007 Brilliant whiteness in ultrathin beetle scales. *Science* **315**, 348. (doi:10.1126/science.1134666)
8 Staude, I., Thiel, M., Essig, S., Wolff, C., Busch, K., von Freymann, G. & Wegener, M. 2010 Fabrication and characterization of Silicon woodpile photonic crystals with a complete bandgap at telecom wavelengths. *Opt. Lett.* **35**, 1094–1096. (doi:10.1364/OL.35.001094)
9 Fischer, J. & Wegener, M. 2011 Three-dimensional direct laser writing inspired by stimulated-emission-depletion microscopy. *Opt. Mater. Express.* **1**, 614–624. (doi:10.1364/OME.1.000614)
10 Noda, S., Tomoda, K., Yamamoto, N. & Chutinan, A. 2000 Full three-dimensional photonic bandgap crystals at near-infrared wavelengths. *Science* **289**, 604. (doi:10.1126/science.289.5479.604)
11 Ozin, G. A. & Yang, S. M. 2001 The race for the photonic chip: colloidal crystal assembly in silicon wafers. *Adv. Funct. Mater.* **11**, 95–104. (doi:10.1002/1616-3028(200104)11:2<95::AID-ADFM95>3.0.CO;2-O)
12 Galusha, J. W., Richey, L. R., Jorgensen, M. R., Gardner, J. S. & Bartl, M. H. 2010 Study of natural photonic crystals in beetle scales and their conversion into inorganic structures *via* a sol–gel bio-templating route. *J. Mater. Chem.* **20**, 1277–1284. (doi:10.1039/B913217A)
13 Gansel, J. K., Thiel, M., Rill, M. S., Decker, M., Bade, K., Saile, V., von Freymann, G., Linden, S. & Wegener, M. 2009 Gold helix photonic metamaterial as broadband circular polarizer. *Science* **325**, 1513–1515. (doi:10.1126/science.1177031)
14 Man, W., Megens, M., Steinhardt, P. J. & Chaikin, P. M. 2005 Experimental measurement of the photonic

properties of icosahedral quasicrystals. *Nature* **436**, 993–996. (doi:10.1038/nature03977)
15 Vukusic, P. & Stavenga, D. G. 2009 Physical methods for investigating structural colours in biological systems. *J. R. Soc. Interface* **6**(Suppl. 2), S133–S148. (doi:10.1098/rsif.2008.0386.focus)
16 Michielsen, K. & Stavenga, D. G. 2008 Gyroid cuticular structures in butterfly wing scales: biological photonic crystals. *J. R. Soc. Interface* **5**, 85–94. (doi:10.1098/rsif.2007.1065)
17 Chin, J. & Coveney, P. V. 2006 Chirality and domain growth in the gyroid mesophase. *Proc. R. Soc. A* **462**, 3575–3600. (doi:10.1098/rspa.2006.1741)
18 Michielsen, K., De Raedt, H. & Stavenga, D. G. 2010 Reflectivity of the gyroid biophotonic crystals in the ventral wing scales of the Green Hairstreak butterfly, *Callophrys rubi*. *J. R. Soc. Interface* **46**, 765–771. (doi:10.1098/rsif.2009.0352)
19 Saba, M., Thiel, M., Turner, M. D., Hyde, S. T., Gu, M., Grosse-Brauckmann, K., Neshev, D. N., Mecke, K. & Schröder-Turk, G. E. 2011 Circular dichroism in biological photonic crystals and cubic chiral nets. *Phys. Rev. Lett.* **106**, 103902. (doi:10.1103/PhysRevLett.106.103902)
20 Saranathan, V., Osuji, C. O., Mochrie, S. G. J., Noh, H., Narayanan, S., Sandy, A., Dufresne, E. R. & Prum, R. O. 2010 Structure, function, and self-assembly of single network gyroid ($I4_132$) photonic crystals in butterfly wing scales. *Proc. Natl Acad. Sci. USA* **107**, 11 676–11 681. (doi:10.1073/pnas.0909616107)
21 Vukusic, P. & Sambles, R. 2001 Shedding light on butterfly wings. *Proc. SPIE* **4438**, 85–95. (doi:10.1117/12.451481)
22 Prum, R. O., Quinn, T. & Torres, R. H. 2006 Anatomically diverse butterfly scales all produce structural colours by coherent scattering. *J. Exp. Biol.* **209**, 748–765. (doi:10.1242/jeb.02051)
23 Michielsen, K. & Kole, J. S. 2003 Photonic band gaps in materials with triply periodic surfaces and related tubular structures. *Phys. Rev. B* **68**, 115 107–115 113. (doi:10.1103/PhysRevB.68.115107)
24 Sambles, J. R., Kelly, R. & Yang, F. 2006 Metal slits and liquid crystals at microwave frequencies. *Phil. Trans. R. Soc. A* **364**, 2733–2746. (doi:10.1098/rsta.2006.1850)
25 High-frequency structure simulator version 13, Finite-element package, Ansoft Corporation, Pittsburgh, PA. See http://www.ansoft.com.
26 Wohlgemuth, M., Yufa, N., Hoffman, J. & Thomas, E. L. 2001 Triply periodic bicontinuous cubic microdomain morphologies by symmetries. *Macromolecules* **34**, 6083–6089. (doi:10.1021/ma0019499)
27 García-Santamaría, F., López, C., Meseguer, F., López-Tejeira, F., Sánchez-Dehesa, J. & Miyazaki, H. T. 2001 Opal-like photonic crystal with diamond lattice. *Appl. Phys. Lett.* **79**, 2309. (doi:10.1063/1.1406560)
28 Ho, K. M., Chan, C. T. & Soukoulis, C. M. 1990 Existence of a photonic gap in periodic dielectric structures. *Phys. Rev. Lett.* **65**, 3152–3155. (doi:10.1103/PhysRevLett.65.3152)
29 Vukusic, P., Sambles, J. R., Lawrence, C. R. & Wootton, R. J. 1999 Quantified interference and diffraction in single Morpho butterfly scales. *Proc. R. Soc. Lond. B* **266**, 1403–1411. (doi:10.1098/rspb.1999.0794)
30 Vukusic, P. & Sambles, J. R. 2003 Photonic structures in biology. *Nature* **424**, 852–855. (doi:10.1038/nature01941)
31 Poladian, L., Wickham, S., Lee, K. & Large, M. C. J. 2009 Iridescence from photonic crystals and its suppression in butterfly scales. *J. R. Soc. Interface* **6**(Suppl. 2), S233–S242. (doi:10.1098/rsif.2008.0353.focus)
32 Trzeciak, T. M. & Vukusic, P. 2009 Photonic crystal fiber in the polychaete worm *Pherusa* sp. *Phys. Rev. E* **80**, 061908. (doi:10.1103/PhysRevE.80.061908)